Title

Scaling of oscillatory kinematics and Froude efficiency in baleen whales

Authors and Affiliations:

Hayden J. Smith[1,2], *William T. Gough[1], Matthew S. Savoca[1], Max F. Czapanskiy[1], Frank E. Fish[3], Jean Potvin[4], K.C. Bierlich[5], David E. Cade[1,6], Jacopo Di Clemente[7], John Kennedy[4], Paolo Segre[1], Andrew Stanworth[8], Caroline Weir[8], Jeremy A. Goldbogen[1]

[1]Hopkins Marine Station, Stanford University, Pacific Grove, CA, [2]Southwestern University, Georgetown, TX, [3]West Chester University, West Chester, PA, [4]Saint Louis University, Saint Louis, MO, [5]Duke University, Durham, NC, [6]University of California Santa Cruz, Santa Cruz, CA, [7]Department of Biology, University of Copenhagen, Copenhagen, Denmark, [8]Falklands Conservation, Stanley, Falkland Islands

*Corresponding Author

Key Words:

Cetacean, Swimming, Hydrodynamics, Thrust, Efficiency

Running Title

Scaling of Cetacean Swimming Efficiency

Summary Statement

We used tags attached to baleen whales to demonstrate how thrust power output, drag coefficient, and Froude efficiency scale with swimming speed and body length.

Abstract

High efficiency lunate-tail swimming with high-aspect-ratio lifting surfaces has evolved in many vertebrate lineages, from fish to cetaceans. Baleen whales (Mysticeti) are the largest swimming animals that exhibit this locomotor strategy and present an ideal study system to examine how morphology and the kinematics of swimming scale to the largest body sizes. We used data from whale-borne inertial sensors coupled with morphometric measurements from aerial drones to calculate the hydrodynamic performance of oscillatory swimming in six baleen whale species (fin whale, *Balaenoptera physalus*; Bryde's whale, *Balaenoptera* edeni; sei whale, *Balaenoptera* borealis; Antarctic minke whales, *Balaenoptera bonaerensis*; humpback whales, *Megaptera novaeangliae*; and blue whales, *Balaenoptera musculus*) ranging in body length from 5-25m. We find that mass-specific thrust increases with both swimming speed and body size. Froude efficiency, defined as the amount of mechanical work the animal does to propel itself forward, increased with swimming speed to a plateau but decreased with body size. This finding

is contrary to previous data for smaller animals that Froude efficiency is positively related to body size. Although our empirically parameterized estimates for the drag of a swimming baleen whale was higher than a simple gliding model, oscillatory locomotion at this scale exhibits high Froude efficiency as in other adept swimmers. Our results quantify the fine-scale kinematics and hydrodynamics of routine and energetically expensive swimming modes at the largest scale.

Introduction

The repeated invasion of aquatic and marine environments by tetrapods over the last 250 million years has resulted in a host of convergent morphological adaptations that facilitate life in water (Kelley & Pyenson, 2015). Among these adaptations are the evolution of a fusiform body shape, flattened control surfaces, and sickle-shaped caudal fin to achieve high performance locomotion (Fish et al., 2008). These morphological adaptations are functionally analogous with other swimming animals such as thunniform fish, lamnid sharks, cetaceans, and the extinct ichthyosaurs (Motani, 2002; Donley et al., 2004; Gleiss et al., 2011). The majority of these swimmers use an oscillatory swimming style that involves side-to-side or up-and-down movement of a hydrofoil-like tail to generate lift-based thrust and overcome drag (Fish, 1998). Cetaceans are unique among oscillatory swimmers because of their extreme body mass, exemplified in modern baleen whales (Mysticeti), which evolved massive body sizes within the last five million years (Slater et al., 2017).

Although the swimming performance of large whales has long been of interest to researchers (Krogh, 1934; Kermack, 1948; Bose & Lien, 1989), direct measures of their swimming kinematics and morphology have been difficult to obtain. Studies of cetacean

swimming kinematics have typically focused on smaller and highly maneuverable odontocete species in captivity (Fish, 1993; Curren et al., 1994; Fish, 1998). Attempts to study mysticetes have been constrained to breathing events at the water's surface. Energetic assumptions (Sumich, 1983; Parry, 1949; Blix & Folkow, 1995) and morphological measurements were limited to deceased animals that had stranded on beaches or been captured by whaling operations (Lockyer, 1976; Kahane-Rapport & Goldbogen, 2018). The recent development of high-resolution biologging methods now allows researchers to quantify the kinematics of free-swimming cetaceans in their natural habitats (Johnson & Tyack, 2003; Goldbogen et al., 2017a; Gough et al., 2019). In addition, unoccupied aircraft systems (UAS, or drone) technology has enhanced our ability to obtain precise morphological data, thereby enabling comparative and scaling analyses of form and function (Kahane-Rapport et al., 2020; Gough et al., 2019).

Understanding the size-dependent kinematics of swimming cetaceans is critical to analyze their swimming performance and energetics. The dorso-ventral oscillation of the flukes produces lift that is resolved into a forward thrust vector (Fig. 1; Lighthill, 1971; Chopra and Kambe, 1977; Vogel, 1994; Fish, 1998). This lift-based thrust power is equal to the drag power of the animal when swimming at a constant velocity (Lighthill, 1971; Fish, 1998). This mechanism is considered to be highly efficient (>75%; Triantafyllou et al., 1991; Rohr & Fish, 2004). Previous attempts to estimate the thrust power of actively swimming large whales have been made based on a number of assumptions without reliable kinematic data (Parry, 1949; Chopra & Kambe, 1977; Yates, 1983; Bose & Lien, 1989). Thrust power generation is modulated through the adjustment of basic kinematic parameters of the oscillatory tailbeat cycle, and new biologging tags make these empirical measurements possible for large, free-swimming animals.

Kinematic studies performed on cetaceans have focused on the three fundamental parameters of an oscillatory tailbeat cycle: amplitude of heave, swimming speed, and oscillatory frequency. Among these, speed has been studied most extensively. Using various methods, researchers have found that many different species of cetaceans are able to swim over an extended range of speeds. High speeds in excess of 8 m/s have been achieved by rorqual mysticetes (Fish & Rohr, 1999; Hirt et al., 2017; Segre et al., 2020). A recent study by Gough et al. (2019) has shown that mysticetes tend to swim at ~2 m/s when they are not feeding. In order to swim at different speeds within this wide range, mysticetes must adjust either their oscillatory frequency or the amplitude of heave (Lighthill, 1971; Chopra & Kambe, 1977). For small odontocetes, Fish (1998) found that oscillatory frequency increased with increasing swimming speed but decreased roughly with body length while amplitude of heave remained constant at ~0.2 of an animal's body length. These findings were recently confirmed for mysticetes by Gough et al. (2019).

Measuring the fundamental kinematic parameters of the oscillatory tailbeat cycle has allowed researchers to estimate Froude efficiency, or the percentage of thrust that is successfully transferred into forward motion (Vogel, 1994; Fish, 1998). The dimensionless Strouhal number has typically been used as a rough way to describe how the amplitude of heave, swimming speed, and oscillatory frequency are modulated and interact to provide a maximally efficient pattern of vorticity around the tail during swimming (Triantafyllou et al., 1991; Fish, 1998; Taylor et al., 2003; Rohr & Fish, 2004; Gough et al., 2019). The generally accepted rule is that highly-efficient oscillatory swimming falls within a Strouhal range from 0.25-0.35 (Triantafyllou et al., 1991). Both Rohr & Fish (2004) and Gough et al. (2019) found that cetaceans fall within this range, but a more detailed analysis of the kinematics and hydrodynamic parameters, such as

the thrust power output and drag, has only been performed previously by Fish (1998) for much smaller odontocetes.

Here, our goal is to move beyond the Strouhal number and use a combination of whale-borne tags and UAS morphological measurements to calculate the kinematics, thrust power output, and Froude efficiencies for free-swimming mysticete whales using similar methods to Fish (1998). Apart from Gough et al. (2019), we have a very limited understanding of how kinematics affect swimming performance at the upper extremes of body size. Previous studies have estimated the Froude efficiency of swimming for odontocetes and other oscillatory swimming animals to be approximately ~75-90% (Fish, 1998), but the only estimate for a mysticete before our study came from a single fin whale (*Balaenoptera physalus*) of unknown body size swimming at ~8 m/s (Bose & Lien, 1989). Our current data set goes beyond any previous analyses and includes six species and a ~5x range in body length. All of the species included in our study are lunge feeders that feed by opening their mouth and engulfing a large volume of water into a highly expansible throat pouch (Goldbogen et al., 2017b). This behavior requires the efficient achievement of high swimming speeds in order to maintain a favorable energetic balance (Potvin et al., 2009). We hypothesize that the kinematic and hydrodynamic parameters of swimming scale similarly between small and large cetaceans and will lead to high (>75%) Froude efficiencies for even the largest animals. Our study will lead to a more complete scaling-based understanding of oscillatory swimming in mysticetes and the kinematic, hydrodynamic, and morphological factors that impact swimming performance in the world's largest animals.

Methods

Study species and locations

The whales included in this study are the Antarctic minke whale (*Balaenoptera bonaerensis*, Burmeister, 1867), humpback whale (*Megaptera novaeangliae*, Borowski, 1781), fin whale (*Balaenoptera physalus*, Linnaeus, 1758), Bryde's whale (*Balaenoptera* edeni, Anderson, 1879), sei whale (*Balaenoptera borealis*, Lesson, 1828), and blue whale (*Balaenoptera musculus*, Linnaeus, 1758). The six species are members of the family Baleanoptera, commonly referred to as rorquals, and tend to have similar life histories and behaviors. These species range in size from ~5 m in length for the Antarctic minke whale up to ~25 m for an adult blue whale (Goldbogen et al., 2019). Distinct morphological differences are also present between these species, with the most prominent being the enlarged flukes and flippers of the humpback whale relative to body size (Fish & Battle, 1995; Woodward et al., 2006).

Data on foraging and swimming was collected on humpback whales off of the coast of Monterey, CA and the Western Antarctic Peninsula, blue whales off California (Monterey Bay and Southern California Bight), Antarctic minke whales off the western Antarctic Peninsula, fin whales in Monterey Bay and the fjords of southeastern Greenland, Bryde's whales off the southern coast of South Africa, and sei whales near the Falkland Islands**.** All work was performed under suitable permits and in accordance with university IACUC procedures (See Acknowledgements section below).

CATS Tags

The Customized Animal Tracking Solutions (CATS) tags integrate video with 400 Hz accelerometers and gyroscopes; 50 Hz magnetometers, pressure and temperature sensors; a 10

Hz internal temperature sensor; and 10 Hz light and GPS sensors. Tag accelerometers for all whales were sampled at 40 or 400 Hz, magnetometers and gyroscopes at 40 or 50 Hz, and pressure, light, temperature, and GPS at 10 Hz. All data were decimated to 10 Hz, tag orientation on the animal was corrected for, and animal orientation was calculated using custom-written scripts in Matla 2014a (following Johnson & Tyack, 2003; Cade et al., 2016). Animal speed for all deployments was determined using the amplitude of tag vibrations (Cade et al., 2018). Tags were deployed from rigid-hull inflatable boats using a 6 m carbon-fiber pole. Tags attached to the animal with four suction cups, detached after suction failed, floated to the surface and were recovered via VHF telemetry. Deployment lengths in this study ranged from 8 mins to 26 hrs. For more information on the tags used in this study, see Goldbogen et al. (2017a).

UAS Operations and *Morphometric Measurements*

Images of each species were collected using UAS between 2017 and 2019. Specifically, two types of stock-build quadcopters, the Phantom 3 and Phantom 4 Pro, as well as two types of custom hexacopters were used, the FreeFly Alta 6 and a Mikrokopter-based LemHex-44. Both quadcopters used stock-built barometers and cameras while the hexacopters contained a 2-axis gimbal fitted with a Lightware SF11/C laser altimeter and a Sony Alpha A5100 camera with an APS-C sensor (23.5 mm by 15.6 mm), 6000 x 4000 pixel resolution, and either a Sony SEL 50 mm or SEL 35 mm focal length low distortion lens.

ImageJ 1.5i (Schindelin et al., 2012) was used to measure the total length, maximum body diameter, fluke chord length, and fluke area (Fig. 2). Measurement errors for each aircraft were estimated by measuring a known sized object floating at the surface from various altitudes,

and each aircraft had an average error < 5%. Measurements in pixels were multiplied by the ground sampling distance (GSD) to convert to meters following Fearnbach et al. (2012):

$$L = n_{pix} \times GSD \quad (1)$$

$$GSD = \frac{a}{l_{foc}} \times \frac{S_W}{P_w} \quad (2)$$

where *L is the length (m),* n_{pix} is the number of pixels, a is the altitude, l_{foc} is the focal length (mm), S_w is the sensor width (mm), and P_w is the image resolution width (px). The width of the sensor and image resolution was used since images of the whales were captured full frame widthwise (Gough et al., 2019). In ImageJ (NIH), the combined planar surface area of the flukes (F_a; m^2) was calculated by carefully drawing a polygonal outline of the flukes. Chord length of the flukes (C; m) was measured as the linear distance from the notch between the flukes to the anterior insertion of the flukes on the tail. Body mass (kg) was estimated from total body length using known regressions (Kahane-Rapport & Goldbogen, 2018). The wetted surface area of the body (S_a ;m^2) was estimated from total body length using data provided by Fish (1993).

Thrust Power, Efficiency, and Drag Coefficient Modeling

We used a customized MATLAB script to detect tailbeat cycles based upon methods defined by Gough et al. (2019). In particular, a series of thresholds were used to define periods in the filtered (low-pass) gyroscope signal (along the transverse axis) corresponding to individual tailbeats. These thresholds checked for symmetricality between the upstroke and downstroke by defining the magnitude, duration, and overall shape of each portion of the tailbeat cycle. The resulting set of tailbeat cycles was spot-checked and compared against tag video to ensure that

206 the parameters were set correctly. Individual whales must have had a dataset of >200 tailbeats in
207 order to be included for further analysis.
208 For each tailbeat, we measured the mean swimming velocity (U; m s^{-1}) by averaging
209 across the entire time course of the cycle. Since the measurement of speed by the tag requires
210 turbulent flow, we were limited to only measure speeds >1 m s^{-1} (Cade et al., 2018). We also
211 measured oscillatory frequency (f; Hz) as the inverse of the duration of the cycle. Our
212 calculations of thrust power (P_T), coefficient of drag (C_D), and Froude efficiency (η) were based
213 on a model of lunate tail propulsion using unsteady wing lifting surface theory (Chopra &
214 Kambe, 1977; Yates, 1983; Fish, 1998). This model begins with the estimation of two input
215 parameters, namely the reduced frequency (σ) defined as:
216
217 $$\sigma = \frac{\omega\, C}{U} \quad (3)$$
218 where ω is the angular frequency of fluking (with $\omega = 2\pi f$); and the feathering parameter (θ)
219 defined as:
220
221 $$\theta = \frac{\alpha\, U}{\omega\, h_1} \quad (4)$$
222 which is expressed as the ratio of the maximum angle (α, in degrees) between the fluke and the
223 direction of motion and the maximum angle ($\omega h_1/U$) achieved by the trajectory of the pitching
224 axis of the flukes (Yates, 1983) when reaching the heave amplitude h_1 *(m)*. We were unable to
225 measure precise values for the α or h_1 from the tag data and instead relied on validated estimates
226 of 30° for α and one-fifth of body lengh for h_1 (Bainbridge, 1958; Fish, 1998).

The model devised by Chopra & Kambe (1977) yielded a series of parametric curves expressing C_T and η in terms of σ and θ (Yates, 1983). We digitized these curves and estimated both values for each tailbeat cycle. We then estimated the mean thrust force ($\bar{T}$) (over a tailbeat cycle), given the relationship:

$$\bar{T} = 0.5\,\rho\,C_T\,u^2\,F_a\left(\frac{h_1}{C}\right)^2 \quad (5)$$

where ρ is the density of seawater, S_t is the fluke area, and *c* is the chord length of the tail from insertion to tail tip. The (mechanical) thrust power output (P_T) is given by:

$$P_T = 0.5\,\rho\,C_T\,U^3\,F_a\left(\frac{h1}{C}\right)^2 \quad (6)$$

and equating the mechanical power generated with the drag power dissipated by the body yields the (mean) drag force and its corresponding drag coefficient: (Fish, 1993):

$$C_D = \frac{P_T}{0.5\,\rho\,S_a\,U^3} \quad (7)$$

Routine vs. Lunge-Associated Swimming

Foraging lunges were detected manually using a series of defined parameters that have been validated using tag video (Cade et al., 2016). These events typically involve an increase in speed followed by a rapid deceleration as the animals opens its mouth (Potvin et al., 2009; Goldbogen et al., 2011; Cade et al., 2016). We chose to define the period from 10-0 seconds prior to the lunge deceleration as the lunge-associated period and any tailbeat that occurred

within that time was similarly classified as lunge-associated. All other tailbeats were classified as routine swimming. The lunge-associated tailbeats likely included a greater change in swimming velocity, but our tailbeat detection thresholds ensured general consistency in the overall kinematic profile of the tailbeats and resulted in two sets of tailbeats at different levels of swimming effort.

Comparison to a Simple Rigid-Body Model

Cetacean swimming involves body and tail heaving motions that are altogether absent with the motions of rigid bodies (e.g., submarines) and significantly increase drag (Fish, 1993; Fish, 1998; Fish & Rohr 1999). We compared our drag coefficient data with that of airship models tested in wind tunnels, as summarized in the following correlation (Hoerner, 1965; Blevins, 1984; Webb, 1975; Kooyman, 1989):

$$C_D = \left[\frac{0.072}{(Re)^{\frac{1}{5}}}\right]\left[1 + 1.5\left(\frac{W_{max}}{L_{body}}\right)^{\frac{3}{2}} 7.0\left(\frac{W_{max}}{L_{body}}\right)^{3}\right] \quad (8)$$

where W_{max} is the maximum body diameter (m). This equation is expressed in terms of the Reynold's number:

$$Re = \frac{L_{body}\, U}{v} \quad (6)$$

in which v is the kinematic viscosity. In this case the drag force ($F_{drag}^{parasite}$) sustained by the airship (or non-tail-heaving whale) is given by:

$$F_{drag}^{parasite} = \frac{1}{2}\,\rho\, S_a\, C_D(t)\, U(t) \quad (10)$$

Statistical Analyses

We compared hydrodynamic performance variables (thrust power output, drag coefficient, and Froude efficiency) with swimming speed, Reynolds number and morphometric measurements using R v. 3.6 and RStudio (Version 1.2.1335, packages: ggpubr, and tidyverse) (R Core Team, 2014; Wickham et al., 2019; Kassambara, 2020). We fit linear models to assess relationships using package lm in R. For our analysis of swimming speed vs Froude efficiency, we used a generalized additive model (GAM) in R (y ~ s[x, bs = "cs"]).

Results

Kinematic and Morphometric Summary

We investigated interspecific relationships between 68 animals and found that mean (± se) values for oscillatory frequency (Hz) and swimming speed (m s^{-1}) both increased when transitioning from routine to lunge-associated swimming. The mean increase in swimming speed between the two modes was 0.695 ± 0.152 m s^{-1} and the mean increase in oscillatory frequency was 0.09 ± 0.02 Hz.

We found that the mean oscillatory frequency for the three species with the most data (humpback, blue, Antarctic minke) decreased with increasing body length with the Antarctic minke whale having the highest values (routine: 0.40 ± 0.010 Hz; lunge-associated: 0.49 ± 0.008 Hz), followed by the humpback whale (routine: 0.24 ± 0.006 Hz; lunge-associated: 0.34 ± 0.011 Hz) and the blue whale (routine: 0.19 ± 0.004 Hz; lunge-associated: 0.24 ± 0.004 Hz). We found

293 that Bryde's and fin whales had similar routine oscillatory frequencies as the humpback whale
294 while having longer average body lengths (Bryde's: 12.04 ± 2.07 m; fin: 18.90 ± 0.43 m) than
295 the humpback whales in our study (11.09 ± 0.33 m). Both of the oscillatory frequency values for
296 the lone tagged sei whale (routine: 0.22 Hz; lunge-associated: 0.30 Hz) fell approximately
297 halfway between the values for the humpback and blue whales, which aligns with the sei whale's
298 body length (16.62 m) being approximately halfway between the mean humpback and blue
299 whale (22.50 ± 0.32 m) body lengths. We found that the oscillatory frequency decreases as the
300 total length increases. We found significant negative relationships between oscillatory frequency
301 and body size during both routine and lunge-associated swimming (routine: $\hat{y}$ = -0.560x + 0.313;
302 R^2 = 0.77; p < 0.001; lunge-associated: $\hat{y}$ = -0.565x + 0.009; R^2 = 0.76; p < 0.001; Fig. 3A).
303 The mean values for both routine and lunge-associated swimming speeds were similar for
304 the humpback (routine: 2.15 ± 0.066 m s^{-1}; lunge-associated: 2.85 ± 0.100 m s^{-1}), blue (routine:
305 2.27 ± 0.063 m s^{-1}; lunge-associated: 3.05 ± 0.056 m s^{-1}), and Antarctic minke whales (routine:
306 2.44 ± 0.053 m s^{-1}; lunge-associated: 2.96 ± 0.117 m s^{-1}). Despite low sample sizes, the average
307 routine and lunge-associated swimming speeds for the Bryde's whale (routine: 1.76 ± 0.51 m s^{-1};
308 lunge-associated: 3.11 ± 0.629 m s^{-1}) and the routine swimming speed for the sei whale (2.23 m
309 s^{-1}) aligned with the humpback, blue, and Antarctic minke whales, while the lunge-associated
310 swimming speed for the sei whale (2.46 m $s^{-1)}$ was lower than other values and both swimming
311 speeds were higher for the fin whale (routine: 3.02 ± 0.125 m s^{-1}; lunge-associated: 3.61 ± 0.900
312 m s^{-1}). We found that swim speed stays fairly constant as the total length increases. Our
313 statistical analysis found no effect of body size on swim speed for both routine and lunge-
314 associated swimming (routine: $\hat{y}$ = -0.003x + 0.785; R^2 = 6.25*10^{-5} ; p = 0.949; lunge-associated:
315 $\hat{y}$ = 0.078x + 0.873; R^2 = 0.04; p = 0.098; Fig. 3B). All species-level means (± se) for each of our

316 measured kinematic and morphometric variables are given in Table 1. The equations and
317 statistics pertaining to our models are given in Table 2.
318
319 *Mass-Specific Thrust Power Output*
320 Among the three species with a large amount of data in our dataset (humpback, blue, and
321 Antarctic minke whales), the humpback whale had the lowest mean mass-specific thrust power
322 output (0.30 ± 0.023 Watts kg^{-1}), with the Antarctic minke whale having a slightly higher value
323 (0.36 ± 0.028 Watts kg^{-1}) and the blue whale having the highest value (0.48 ± 0.025 Watts kg^{-1}).
324 The Bryde's (0.50 ± 0.213 Watts kg^{-1}), sei (0.51), and fin whale (0.74 ± 0.130 Watts kg^{-1}) each
325 had higher values.
326 We found that mean mass-specific thrust power output increased with the transition from
327 routine to lunge-associated swimming modes (Fig. 4A-B). There was a positive effect of
328 swimming speed on mass-specific thrust power output during both routine and lunge-associated
329 swimming (routine: $\hat{y} = 731x - 2.764$; $R^2 = 0.40$; $p < 0.001$; lunge-associated: $\hat{y} = 0.630x -$
330 2.138; $R^2 = 0.49$; $p < 0.001$; Fig 4A). We also found that mean mass-specific thrust power output
331 increases with body length for both routine ($\hat{y} = 0.033x - 1.594$; $R^2 = 0.23$; $p < 0.001$) and lunge-
332 associated swimming ($\hat{y} = 0.031x - 0.693$; $R^2 = 0.16$; $p < 0.001$; Fig. 4B). The species-level
333 means (± se) for each of our measured hydrodynamic parameters are given in Table 3.
334
335 *Drag Coefficient*
336 Among humpback, blue, and Antarctic minke whales, the Antarctic minke whale had the
337 lowest mean drag coefficient (0.01 ± 0.001), with the humpback whale slightly higher ($0.02 \pm$
338 0.002) and the blue whale having the highest value (0.04 ± 0.006). We found that the drag

coefficient for both routine and lunge-associated swimming decreased with increasing swim speed (routine: $\hat{y}$ = - 0.613x – 2.617; R^2 = 0.12; p = 0.004; lunge-associated: $\hat{y}$ = -0.270x – 3.148; R^2 = 0.06; p = 0.042; Fig 5A). Conversely, we found that the drag coefficient increased for both routine and lunge-associated swimming with increasing total body length (routine: $\hat{y}$ = 0.082x – 5.080; R^2 = 0.64; p < 0.001; lunge-associated: $\hat{y}$ = 0.058x – 4.737; R^2 = 0.41; p < 0.001; Fig 5B).

We found that the drag coefficient increased significantly with Reynolds number (routine: $\hat{y} = 2.92*10^{-8}x - 4.805$; R^2 = 0.41; p < 0.001; lunge-associated: $\hat{y} = 1.36*10^{-8}x - 4.476$; R^2 = 0.23; p < 0.001; Fig 5C). In comparison to the R-100 rigid-hulled airship model, all species displayed higher drag coefficients for both swimming modes (Fig 5C).

Froude Efficiency

Of the three species with a large quantity of data in our dataset (humpback, blue, and Antarctic minke whales), the Antarctic minke whale had the highest mean Froude efficiency (0.920 ± 0.004), with the humpback having a lower mean value (0.908 ± 0.003) and the blue whale having the lowest mean value (0.860 ± 0.006). The mean values for the Bryde's (0.868 ± 0.022), sei (0.876), and fin whales (0.889 ± 0.018) were all near the low end of the range.

We found that mean Froude efficiency increases with increasing swimming speed up to a plateau at ~3 m s^{-1} and began to drop off at 5 m s^{-1} for lunge-associated tailbeats (Fig. 6A). On the other hand, we found that mean Froude efficiency decreased with increasing body length (routine: $\hat{y}$ = -0.004x – 0.049; R^2 = 0.68; p < 0.001; lunge-associated: $\hat{y}$ = -0.003x – 0.068; R^2 = 0.47; p < 0.001; Fig. 6B). As compared to prior studies, our results demonstrate that, regardless of body size, rorqual whales demonstrate high efficiency (>75%) comparable to other oscillatory swimmers (Fig. 7). Sub-carangiform, undulatory swimmers such as the rainbow trout

(*Oncorhynchus mykiss*) are slightly lower (~60-80%) and drag-based swimmers, such as the muskrat and human, have much lower Froude efficiencies (~20-35%) (Fig. 7). Table 4 gives additional information about each literature-based mean Froude efficiency value.

Discussion:

Many previous studies that have quantified the kinematics and hydrodynamics of cetacean swimming have used captive animals that can be measured reliably from a stable reference position (Fish, 1993; Fish, 1998; Rohr & Fish, 2004). By comparison, the present study is a first approximation for many of the same kinematic variables of much larger species in their natural environment. Several parameters, such as the angle of attack of the flukes relative to the body or the amplitude of heave are still generally unknown (except in rare circumstances, see Gough et al., 2019), so we supplemented our empirical data with validated estimates for these unknown variables (Bainbridge, 1958; Fish, 1998). The angle of attack of the fluke has been found to change with speed over a range from 20-40°, so we used 30° as an average value (Fish, 1998). Amplitude of heave has been reliably measured as one-fifth of body length and remains constant across swimming speeds and body size (Bainbridge, 1958; Fish, 1998). Our combination of empirical measurements and reliable estimates allowed us to quantify hydrodynamic and kinematic aspects of mysticete swimming using a numerical computation based on unsteady lifting-surface theory and derived by Chopra & Kambe (1977), which has also been validated for odontocetes by Fish (1998). The similarity between our methods and those of previous studies extends our ability to compare swimming performance across vast body size ranges.

385

386 *Oscillatory Frequency and Swimming Speed*

387 Our results illustrate that the transition from routine to lunge-associated swimming
388 predictably results in increased oscillatory frequencies and swimming speeds as the animal
389 prepares for a lunge (Fig. 3) (Goldbogen et al., 2011; Cade et al., 2016). Gough et al. (2019)
390 found that the oscillatory frequency decreases with increasing body size to the power of -0.53,
391 and with a more robust data set we have found a similar scaling exponent of -0.48. For
392 swimming speed, we again found similar results to Gough et al. (2019) with swimming speed
393 remaining consistent at ~2 m s^{-1}. For both oscillatory frequency and swimming speed, the scaling
394 exponents for routine and lunge-associated swim efforts were nearly identical, with a difference
395 of 0.006 for oscillatory frequency and a difference of 0.001 for swimming speed. This suggests
396 that, regardless of body size, mysticetes prepare for a feeding lunge through similar kinematic
397 pathways which include a consistent increase in both oscillatory frequency and swimming speed.
398 These results for oscillatory frequency and swimming speed align with previous results for fish
399 and odontocetes that have shown that swimming speed is heavily modulated by oscillatory
400 frequency (Bainbridge, 1958; Fish, 1998; Gough et al., 2019).

401

402 *Mean Mass-Specific Thrust*

403 Thrust generation is a fundamental aspect of any swimming mode and the achievable
404 thrust for a swimming animal has a direct impact on its maximum swimming speed and,
405 subsequently, the types and quantities of prey that it can capture (Fish, 1998; Potvin et al., 2009;
406 Cade et al., 2020). Hydrodynamic theory states that thrust should increase with the square of
407 velocity (Webb, 1975; Vogel, 1994). Thrust from an oscillating hydrofoil will further increase

408 the thrust of a system by 3-to-5 times (Lighthill, 1971; Liu et al., 1997; Anderson et al., 2001;
409 Fish et al., 2014). While this theory holds for animals of similar sizes, we found it advantageous
410 to measure the mass-specific thrust to make comparisons between mysticetes and other cetaceans
411 that vary across a wide range of body sizes.

412 For cetaceans, high mass-specific thrust allows odontocetes to capture fast-moving,
413 individual fish (Maresh et al., 2004) and allows mysticetes to achieve high speeds during feeding
414 lunges to offset the deceleration during prey engulfment as well as the potential escape response
415 of different prey types (Cade et al., 2016; Cade et al., 2020). Fish (1998) measured the mass-
416 specific thrust of odontocete species and found maximum mass-specific thrust values of 22.5 and
417 23.7 W kg^{-1} for *Pseudorca crassidens* and *Tursiops truncatus*, respectively. The maximum mass-
418 specific thrust value for a mysticete (Bryde's) swimming at 5.7 m s^{-1} in our study was found to
419 be 19.7 W kg^{-1}, but mass-specific thrust values at the species-level averaged between 0.30-0.75
420 W kg^{-1}, which was two orders of magnitude lower (Fig 4A; Table 3). These results suggest that
421 mysticetes typically maintain low average mass-specific thrust values in accordance with their
422 relatively steady swimming speeds (~1.5-2.5 m s^{-1}), but that they can attain extremely high mass-
423 specific thrust power output when properly motivated. Swimming speeds higher than those
424 found in our dataset have also been found for humpbacks (up to ~9 m s^{-1}; Tomilin, 1957; Segre
425 et al., 2020), indicating that they could be producing mass-specific thrust values on par with
426 odontocetes during fast maneuvers such as surface breaches.

427 Our comparisons of speed-matched mass-specific thrust output between routine
428 swimming and lunges suggest that whales likely alter oscillatory frequency in order to generate
429 greater thrust during feeding (Gough et al., 2019). Mass-specific thrust at a routine swimming
430 speed (~1.5-2.5 m s^{-1}) results in a low propulsive energy cost (Gough et al., 2019). The similarity

of the mass-specific thrust increase (~two-fold) from routine to a lunge feeding effort across our range in body size suggests that all of the large whales studied are preparing for a lunge in similar ways. Field data (Cade et al., 2020) and hydrodynamic models (Potvin et al., 2009) suggest that the whales begin lunges at high speeds (3.5-5 m s^{-1}) in order to overcome heightened drag during engulfment and krill-feeders usually move through the prey patch on momentum (Potvin et al., 2009).

Focusing more heavily on the relationship between mass-specific thrust generation and body size, our results diverge slightly from previous estimates. Fish (1998) determined that mass-specific thrust and body size have no relationship. Hill (1950) considered that for similar animals, the maximum power generated during a steady effort would increase not directly with the weight (W), but rather with $W^{0.73}$. As a result, we expected that mass-specific thrust would decrease proportionately with increasing body size. Instead, we found that mass-specific thrust increases as body length increases (Fig. 4). This relationship could result from the higher oscillatory frequencies with larger body sizes that Gough et al. (2019) and our current study found in contrast to previous expectations of oscillatory frequency (Hill, 1950; Sato et al., 2007). For the relationship between oscillatory frequency and body length, Sato et al. (2007) found a more extreme allometric scaling exponent (approximately -1.0), whereas Gough et al. (2019) and our current study found an exponent of approximately -0.5, suggesting a less extreme decrease in oscillatory frequency with increasing body length.

Drag Coefficient vs. Reynolds Number

In comparison to our tagged animals, Hoerner's R-100 airship model used for computational analysis did not include control surfaces (flippers or flukes). Instead, the

approximated environment around the airship was determined using wind tunnel test data (Hoerner, 1965; Blevins, 1984). These modeled values suggest that for an Antarctic minke whale (~5m), the drag coefficients for fluking should be roughly three times higher than non-fluking and gliding. But the difference between these coefficients should increase for larger animals, culminating in a six-fold difference for a blue whale (~22m) (Fig. 6B). Other studies predicted similar increases in the drag coefficient, with Lighthill (1971) first noticing a discrepancy between the expected drag coefficient based on Hoerner's model and the observed values for swimming fish, but his conclusions did not account for changing Reynolds numbers and were based upon animals swimming at Reynolds numbers of $\sim 10^5$ whereas large cetaceans are routinely swimming at values of $\sim 10^7$. Fish (1993) included a variety of species and groups and found higher drag coefficient values for swimming animals as compared to model estimates, but they did not find an increase with increasing Reynolds number like we have for larger cetaceans (Fig. 6C). Fish (1998) analyzed how the drag coefficient might vary with Reynolds number among four species of odontocetes and found that the drag coefficient should decrease with increasing Reynolds number.

For mysticetes, we found a negative relationship between the drag coefficient and the swimming speed as well as a positive relationship between the drag coefficient and body length (Fig. 5A-B). Reynolds number is affected by both the swimming speed and the body length of an animal, so we believe that the impact of body size between individuals is more extreme than the impact of swimming speed within individuals, resulting in a net positive impact of Reynolds number on drag coefficient (Fig. 5C). The effects of swimming speed on drag coefficient have been determined previously by Fish (1998) for a group of odontocetes, but ours is the first study

476 that includes a large enough body size range to be able to parse out the effect of body size on
477 both Reynolds number and drag coefficient.
478
479 *Froude Efficiency vs. Swimming Velocity*
480 Optimal locomotor speeds have been demonstrated for runners, flyers, and swimmers
481 (e.g., Tucker, 1968; Webb, 1975; Hoyt & Taylor, 1981). The cost of transport (COT) has been
482 used as the metabolic proxy that is inversely related to the Froude efficiency (Fish, 2000;
483 Williams et al., 1993) and Yazdi et al. (1999) found that the minimum COT for the bottlenose
484 dolphin (*Tursiops truncatus*) occurred at swimming speeds of 2.1 and 2.5 m s^{-1}, respectively.
485 These speeds coincided with the routine swimming speeds in wild populations. Similarly, gray
486 whales (*Eschrichtius robustus*) and Antarctic minke whales cruise at the speed of the lowest
487 COT (Sumich, 1983; Blix & Folkow, 1995). The minimum COT for the gray whale
488 corresponded to the swimming velocity (2.0-2.5 m s^{-1}) of migrations (Wyrick, 1954; Williamson,
489 1972; Sumich, 1983), which was similar to the velocity of maximum efficiency for whales in the
490 present study. Antarctic minke whales, however, were determined to have a minimum COT at
491 the maximum cruising velocity of 3.25 m s^{-1} (Blix & Folkow, 1995), which was 37% higher than
492 the optimal velocity for maximum Froude efficiency in the present study. However, the velocity
493 of maximum Froude efficiency (2.37 m s^{-1}; current study) was within the range of swimming
494 velocities (1.5-2.6 m s^{-1}) for migrating Antarctic minke whales (Williamson, 1972).
495 Correspondingly, the swimming velocity for maximum Froude efficiency of the blue whale (2.02
496 m s^{-1}) and the humpback whale (2.00 m s^{-1}) were within the ranges of migratory velocities of
497 1.5-3.1 m s^{-1} (Williamson, 1972) and 1.1-4.0 m s^{-1} (Chittleborough, 1953; Williamson, 1972),
498 respectively.

Our results show that Froude efficiency increases rapidly below ~2 m s^{-1} and plateaus, which broadly agrees with the results from Fish (1998) for ontocetes. In contrast with their data, we found that Froude efficiency tapers off above ~5 m s^{-1} during lunge-associated swimming, but not routine swimming. This could be an artifact of our dataset having fewer lunge-associated tailbeats or could suggest a kinematic shift between the two swimming modes – such as a change in the amplitude of heave or angle of attack of the fluke – that is not being accounted for in our estimations. If the latter is true, the whales could be optimizing for another parameter, such as prey capture efficiency or momentum generation, in exchange for a lower Froude efficiency at high speeds.

A reduced Froude efficiency would increase the energetic expenditure when foraging. Such an increase would have consequences to the whale's energy budget and limit dive duration and associated feeding efficiency (Acevedo-Guitteriez et al., 2002; Croll et al., 2005). Compared to the Balaenopteridae, the Balaenidae (i.e., right whales, bowhead whale) swim slowly through the water and maintain a steady speed during ram filter feeding (Burns et al., 1993; Simon et al., 2009). The foraging strategy of the rorquals places greater energetic demands on balaenopteridae than the balaenids (Potvin & Werth, 2016; Potvin & Werth, 2017).

Froude Efficiency vs. Total Body Length (m)

In this study, Froude efficiency relates to the amount of mechanical work the animal does to propel itself forward. Previous research has shown that Froude efficiency would remain constant or slightly increase with increasing body size (Fish, 1998). However, we found that Froude efficiency decreases with increasing body size among rorquals (See Fig. 7B). The mechanistic explanation of this finding is that larger individuals have a slightly increased thrust

522 generation but a greatly increased drag coefficient (Figs. 4 and 6), thus resulting in a lower
523 Froude efficiency, because more energy may be required to overcome drag and achieve
524 equivalent locomotor performance.
525 Our analyses suggest that size is an important determinant of swimming performance in
526 rorquals. Balaenopteridae exhibit a size range than spans an order of magnitude in body mass,
527 from Antarctic minke whales to blue whales (Lockyer, 1976). The scale of these ocean giants
528 necessitates the use of oscillatory lift-based swimming as an effective propulsive mechanism for
529 high-speed swimming at high Reynolds numbers (Webb and De Buffrénil, 1990; Fish, 2020).
530 Interestingly in parallel with the trend of maximum speed in which intermediate animals
531 exhibited the highest performance with lower maximum speeds for small and large animals, it
532 was found for whales that Froude efficiency, another locomotor performance variable, decreased
533 above and below an optimal size (Hirt et al., 2017) (Fig. 7; Table 4).
534
535 *Conclusions*
536 Although the thrust power required to achieve maximum speed appears to be constrained
537 at large body sizes, large rorquals may benefit from a low cost of transport (Williams, 1999;
538 Gough et al., 2019). Accordingly, the high burst velocities and accelerations attained by the
539 whales during lunges would incur reduced Froude efficiencies compared to routine and
540 migratory velocities. The reduced Froude efficiency would place increased energetic demands
541 during active foraging using a lunge feeding strategy for the balaenopterids. Our results are some
542 of the first to quantify the fine-scale hydrodynamics that underlie these energetic differences
543 between routine and energetically expensive swimming modes and include some of the largest

absolute body sizes as well as a larger body size range than any previous study on swimming animals.

Acknowledgments:

We thank Malene Simon, Gwenith Penry, Ari Friedlaender, Dave Johnston, Julian Dale, and the Duke University Marine Robotics and Remote Sensing Lab for research support. We would also like to thank the California State University Monterey Bay Research Experiences for Undergraduates (CSUMB REU) team. We are grateful for the cooperation of the Southwestern Physics Department. Thanks to the Shallow Marine Surveys Group for support with boat work in the Falkland Islands. All procedures in USA and Antarctica (14809) were conducted under approval of the National Marine Fisheries Service (Permits 781-1824, 16163, 14809, 16111, 19116, 15271, 20430), Canada DFO SARA/MML 2010-01/SARA-106B, National Marine Sanctuaries (MULTI-2017-007), Research permit R23.2018 issued by the Falkland Islands Government, ACA 2015-014, and institutional IACUC committees.

Competing Interests:

We have no competing interests to report.

Funding:

This research was funded by the National Science Foundation in support of research experiences for undergraduates (REU) to CSUMB. Additionally, this research was funded in part by grants from the National Science Foundation (IOS-1656691, IOS-1656676, IOS-1656656; OPP-1644209), the Office of Naval Research (N000141612477), the World Wildlife Fund, and a Terman Fellowship from Stanford University. Fieldwork in South Africa was funded by Percy Sladen Memorial Trust, Torben og Alice Frimodts grant, PADI foundation and Society of Marine Mammalogy. Additional Monterey Bay CATS tag deployments were funded by grants from the American Cetacean Society Monterey and San Francisco Bay chapters, and by the Meyers Trust. Sei whale work in the Falkland Islands was funded by a Darwin Plus grant (DPLUS082).

References:

1. Acevedo-Gutierrez, Alejandro & Croll, Donald & Tershy, Bernie. (2002). High costs limit dive time in the largest whales. *J. Exp. Biol*. 205: 1747-1753.
2. Anderson, E. J., McGillis, W. R. and Grosenbaugh, M. A. (2001). The boundary layer of swimming fish. *J. Exp. Biol*. **204**: 81-102.
3. Bainbridge, R. (1958). The speed of swimming of fish as related to size and to the frequency and amplitude of the tail beat. *J. Exp. Biol.* **35**: 109-133.
4. Blake, R. W. (1979). The mechanics of labriform locomotion I. labriform locomotion in the angelfish (*Pterophyllum eimekei*): an analysis of the power stroke. *J. Exp. Biol.* **82**: 255–271.

5. Blake, R. W. (1980). The mechanics of labriform locomotion II. an analysis of the recovery stroke and the overall fin-beat cycle propulsive efficiency in the angelfish. *J. Exp. Biol.* **85**: 337–342.
6. Blevins, R. D. (1984). *Applied fluid dynamics handbook*. New York, N.Y: Van Nostrand Reinhold Co.
7. Blickhan, R. and Cheng, J-Y (1994). Energy storage by elastic mechanisms in the tail of large swimmers – a re-evaluation. *J. Theor. Biol.* **168**: 315-321.
8. Blix, A. S. and Folkow, L. P. (1995). Daily energy expenditure in free living minke whales. *Acta Physiol. Scand*. **153**: 61-66.
9. Bose, N. and Lien, J. (1989). Propulsion of a fin whale (*Balaenoptera physalus*): Why the fin whale is a fast swimmer. *P. Roy. Soc. B-Biol. Sci.* **237**: 175–200.
10. Burns, J. J., Montague, J. J. and Cowles, C. J. (1993). *The bowhead whale*. Spec. Publ. No. 2. The Society for Marine Mammalogy.
11. Cade, D. E., Friedlaender, A. S., Calambokidis, J., Goldbogen, J. A. (2016). Kinematic diversity in rorqual whale feeding mechanisms. *Curr. Biol.* **26**: 2617-2624.
12. Cade, D.E., Barr, K. R., Calambokidis, J., Friedlaender, A. S. and Goldbogen, J. A. (2018). Determining forward speed from accelerometer jiggle in aquatic environments. *J. Exp. Biol.* **221**, jeb170449.
13. Cade, D. E., Carey, N., Domenici, P., Potvin, J., and Goldbogen, J. A. (2020) Predator-informed looming stimulus experiments reveal how large filter feeding whales capture highly maneuverable forage fish. *Proc. Nat. Acad. Sci.* **117**: 472-478.

14. Chittleborough, R. G. (1953). Aerial observations on the humpback whales, *Megaptera nodosa* (Bonnaterre), with notes on other species. *Aust. J. Mar.Freshwater Res.* **4**: 219-226.

15. Chopra, M. G. and Kambe, T. (1977). Hydromechanics of lunate-tail swimming propulsion. Part 2. *J. Fluid Mech*. ***79***(1): 49-69.

16. Croll, Donald & Marinovic, Baldo & Benson, Scott & Chavez, Francisco & Black, Nancy & Ternullo, Richard & Tershy, Bernie. (2005). From wind to whales: Trophic links in a coastal upwelling system. Marine Ecology-progress Series - MAR ECOL-PROGR SER. 289. 117-130.

17. Curren, K. C., Bose, N., and Lien, J. (1994). Swimming kinematics of a harbor porpoise (*Phocoena phocoena*) and an Atlantic white- sided dolphin (*Lagenorhynchus acutus*). *Mar. Mamm. Sci.* **10**: 485–492.

18. Donley, J. M., Sepulveda, C. A., Konstantinidis, P., Gemballa, S. and Shadwick, R. E. (2004). Convergent evolution in mechanical design of lamnid sharks and tunas. *Nature.* **429**, 61-65.

19. Fearnbach, H., Durban, J., Parsons, K., and Claridge, D. (2012). Photographic mark–recapture analysis of local dynamics within an open population of dolphins. *Ecol. Appl.* ***22***(5): 1689-1700.

20. Fish, F. E. (1984). Mechanics, power output and efficiency of the swimming muskrat (*Ondatra zibethicus*). *J. Exp. Biol.* **110**: 183-201.

21. Fish, F. E. (1993). Power output and propulsive efficiency of swimming bottlenose dolphins (*Tursiops truncatus*). *J. Exp. Biol.* **185**: 179-193.

631 22. Fish, F. E. (1998). Comparative kinematics and hydrodynamics of odontocete cetaceans:
632 morphological and ecological correlates with swimming performance. *J. Exp. Biol.* **201**:
633 2867-2877.
634 23. Fish, F. E. (2000). Biomechanics and energetics in aquatic and semiaquatic mammals:
635 Platypus to whale. *Physiol. Biochem. Zool*. **73**: 683-698.
636 24. Fish, F. E. (2020). Aquatic animals operating at high Reynolds numbers: Biomimetic
637 opportunities for AUV applications. P.p. In press. In: Bioinspired Design (W. Soboyejp,
638 ed.), Cambridge University Press, Cambridge.
639 25. Fish, F. E. and Battle, J. M. (1995). Hydrodynamic design of the humpback whale
640 flipper. *J. Morph.* **225**, 51-60.
641 26. Fish F. E., Howle, E. L., Murray, M. M. (2008). Hydrodynamic flow control in marine
642 mammals, *Integr. Comp. Biol.* **48**: 788–800.
643 27. Fish, F. E., Innes, S. and Ronald, K. (1988). Kinematics and estimated thrust production
644 of swimming harp and ringed seals. *J. Exp. Biol.* **137**: 157–173.
645 28. Fish, F. E., Legac, P., Williams, T. M. and Wei, T. (2014). Measurement of
646 hydrodynamic force generation by swimming dolphins using bubble DPIV. *J. Exp. Biol.*
647 **217**: 252-260.
648 29. Fish, F.E. and Rohr, J.J. (1999). *Review of dolphin hydrodynamics and swimming*
649 *performance*. *SPAWARS System Center Technical Report* 1801, San Diego, CA.
650 30. Gleiss, A. C., Jorgensen, S. J., Liebsch, N., Sala, J. E., Norman, B., Hays, G.C., Quintana,
651 F., Grundy, E., Campagna, C., Trites, A.W., Block, B.A. and Wilson, R.P. (2011).
652 Convergent evolution in locomotory patterns of flying and swimming animals. *Nature*
653 *Comms.* **2**: 1-7.

31. Goldbogen, J. A., Cade, D. E., Boersma, A. T., Calambokidis, J., Kahane-Rapport, S. R., Segre, P. S., Stimpert, A. K. and Friedlaender, A. S. (2017a). Using digital tags with integrated video and inertial sensors to study moving morphology and associated function in large aquatic vertebrates. *Anat. Rec.* **300**: 1935-1941.

32. Goldbogen, J.A., Cade, D.E., Calambokidis, J., Friedlaender, A.S., Potvin, J., Segre, P.S. & Werth, A.J. (2017b) How Baleen Whales Feed: The Biomechanics of Engulfment and Filtration. *Annual review of marine science,* **9,** 1-20.

33. Goldbogen, J. A., Cade, D. E., Wisniewska, D. M., Potvin, J., Segre, P. S., Savoca, M. S., Hazen, E. L., Czapanskiy, M. F., Kahane-Rapport, S. R., DeRuiter, S. L., Gero, S., Tønnesen, P., Gough, W. T., Hanson, M. B., Holt, M. M., Jensen, F. H., Simon, M., Stimpert, A. K., Arranz, P., Johnston, D. W., Nowacek, D. P., Parks, S. E., Visser, F., Friedlaender, A. S., Tyack, P. L., Madsen, P. T. and Pyenson, N. D. (2019). Why whales are big but not bigger: Physiological drivers and ecological limits in the age of ocean giants. *Science* **366**: 1367-1372.

34. Goldbogen, J. A., Calambokidis, J., Oleson, E., Potvin, J., Pyenson, N. D., Schorr, G., & Shadwick, R. E. (2011). Mechanics, hydrodynamics and energetics of blue whale lunge feeding: efficiency dependence on krill density. *J. Exp. Biol.* **214**: 121-146.

35. Gough, W. T., Segre, P. S., Bierlich, K. C., Cade, D. E., Potvin, J., Fish, F. E., Dale, J., di Clemente, J., Friedlaender A. S., Johnston D. W., Kahane-Rapport, S. R., Kennedy, J., Long J. H., Oudejans, M., Penry, G., Savoca, M. S., Simon, M., Videsen, S. K. A., Visser, F., Wiley, D. N. and Goldbogen, J. A. (2019). Scaling of swimming performance in the largest animals. *J. Exp. Biol.* **222**: jeb204172.

36. Hill, A. V. (1950). The dimensions of animals and their muscular dynamics. *Sci. Prog*. **38**: 209-230.

37. Hirt, M. R., Jetz, W., Rall, B. C. and Brose, U. (2017). A general scaling law reveals why largest animals are not the fastest. *Nat. Ecol. Evol*. **1**: 1116-1122.

38. Hoerner, S. F. (1965). Fluid dynamic drag. Published by author, Midland Park, NJ.

39. Hoyt, D. F. and Taylor, C. R. (1981). Gait and the energetics of locomotion in horses. *Nature* **292**: 239-240.

40. Johnson, M.P. & Tyack, P.L. (2003) A digital acoustic recording tag for measuring the response of wild marine mammals to sound. *IEEE Journal of Oceanic Engineering,* **28,** 3-12.

41. Kahane-Rapport, S. R. and Goldbogen, J. A. (2018). Allometric scaling of morphology and engulfment capacity in rorqual whales. *J. Morph*. **279**: 1256-1268.

42. Kahane-Rapport, S. R., Savoca, M. S., Cade, D. E., Segre, P. S., Bierlich, K. C., Calambokidis, J., Dale, J., Fahlbusch, J. A., Friedlaender, A. S., Johnston, D. W., Werth, A. J. and Goldbogen, J. A. (2020). Lunge filter feeding biomechanics constrain rorqual foraging ecology across scale. *J. Exp. Biol.* **279**, jeb.224196.

43. Kassambara, A. (2020). ggpubr: 'ggplot2' Based Publication Ready Plots. Cran.R-Projects. Version 0.4.0.

44. Kelley, N. and Pyenson, N. (2015). Vertebrate evolution. Evolutionary innovation and ecology in marine tetrapods from the Triassic to the Anthropocene. *Science* **348**: 301-308.

45. Kermack, A. K. (1948). The propulsive powers of blue and fin whales. *J. Exp. Biol.*1948 25: 237-240.

46. Kojeszewski, T. and Fish, F.E. (2007). Swimming kinematics of the Florida manatee (*Trichechus manatus latirostris*): hydrodynamic analysis of an undulatory mammalian swimmer. *J. Exp. Biol.* **210**: 2411–2418.

47. Kooyman, G. L. (1989). Diverse divers: physiology and behavior. Berlin: Springer-Verlag.

48. Krogh, A. (1934). Conditions of life at great depths in the ocean. Ecol. Mongraphs 4: 430-439.

49. Lighthill, J. (1971). Large-amplitude elongate-body theory of fish locomotion. *Proc. R. Soc. B* **179**: 125-138.

50. Liu, H., Wassersug, R. J. and Kawachi, K. (1997). The three-dimensional hydrodynamics of tadpole locomotion. *J. Exp. Biol*. **200**: 2807-2819.

51. Lockyer, C. (1976). Body weights of some species of large whales. *ICES J. Mar. Sci.* **36**: 259-273.

52. Magnuson, J. J. (1978). Locomotion by Scombrid Fishes: Hydromechanics, Morphology, and Behavior. In *Fish Physiology*. 239–313. Elsevier.

53. Maresh, J. L., Fish, F. E., Nowacek, D. P., Nowacek, S. M. and Wells, R. S. (2004). High performance turning capabilities during foraging by bottlenose dolphins (*Tursiops truncatus*). *Mar. Mamm. Sci*. **20**: 498-509.

54. McCutchen, C. W. (1975). Froude propulsive efficiency of a small fish, measured by wake visualization. *Scale effects in animal locomotion.* 339-363. Academic Press London, New York.

55. Motani, R. (2002). Scaling effects in caudal fin propulsion and the speed of ichthyosaurs. *Nature* **415**: 309-312.

56. Parry, D.A. (1949). The swimming of whales and a discussion of Gray's paradox. *J. Exp. Biol.* **26**: 24-28.

57. Potvin, J., Goldbogen, J. A. and Shadwick, R. E. (2009). Passive versus active engulfment: verdict from trajectory simulations of lunge-feeding fin whales Balaenoptera physalus. *J. Roy. Soc. Interf*ace **6**: 1005-1025.

58. Potvin. J. and Werth, A. J. (2016). Baleen hydrodynamics and morphology of cross-flow filtration in balaenid whale suspension feeding. *PLoS ONE* **11**: E0150106.

59. Potvin J. and Werth A. J. (2017). Oral cavity hydrodynamics and drag production in Balaenid whale suspension feeding. *PLoS ONE* 12: e0175220.

60. R Core Team (2014). R: A language and environment for statistical computing. R Foundation for Statistical Computing, Vienna, Austria. URL http://www.R-project.org/.

61. Rohr, J. and Fish, F. E. (2004). Strouhal numbers and optimization of swimming by odontocete cetaceans. *J. Exp. Biol*. **207**: 1633-1642.

62. Schindelin, J., Arganda-Carreras, I., Frise, E., Kaynig, V., Longair, M., Pietzsch, T., Preibisch, S., Rueden, C., Saalfeld, S., Schmid, B. et al. (2012). Fiji: an open-source platform for biological-image analysis. *Nat. Methods* **9**: 676-682.

63. Segre, P. S., Potvin, J., Cade, D. E., Calambokidis, J., Di Clemente, J., Fish, F. E., Friedlaender, A. S., Gough, W. T., Kahane-Rapport, S. R., Oliveira, C., Parks, S. E., Penry, G. S., Simon, M., Stimpert, A. K., Wiley, D. N., Bierlich, K. C., Madsen, P. T. and Goldbogen, J. A. (2020). Energetic and physical limitations on the breaching performance of large whales. *eLife*. **9**: e51760.

64. Simon, M., Johnson, M., Tyack, P., & Peter, M. T. (2009). Behaviour and kinematics of continuous ram filtration in bowhead whales (*Balaena mysticetus*). *Proc. R. Soc. B.***276**3819–3828

65. Slater G. J., Goldbogen J. A. and Pyenson N. D. (2017). Independent evolution of baleen whale gigantism linked to PlioPleistocene ocean dynamics. *Proc. R. Soc. B* **284**: 20170546.

66. Sumich, J. L. (1983). Swimming velocities, breathing patterns, and estimated costs of locomotion in migrating gray whales, *Eschrichtius robustus*. *Can. J. Zool*. **61**: 647-652.

67. Taylor, G. K., Nudds, R. L. and Thomas, A. L. R. (2003). Flying and swimming animals cruise at a Strouhal number tuned for high power efficiency. *Nature.* **425**: 707-711.

68. Tomilin, A.G. (1957). *Mammals of the USSR and Adjacent Countries*. Volume IX, Cetacea. Izdatel'stvo Akademi Nauk SSSR, Moskva (Translated from Russian).

69. Triantafyllou, M. S., Triantafyllou, G. S. and Gopalkrishnan, R. (1991). Wake mechanics for thrust generation in oscillating foils. *Phys. Fluids.* **3**: 2835-2837.

70. Tucker, V. A. (1968). Respiratory exchange and evaporative water loss in the flying budgerigar. *J. Exp. Biol*. **48**: 67-87.

71. Vogel, S. (1994). *Life in Moving Fluids*. Princeton, NJ: Princeton University Press.

72. Von Loebbecke, A., Mittal, R., Fish, F. and Mark, R. (2009). Propulsive efficiency of the underwater dolphin kick in humans. *J. Biomech. Eng.* **131**: 054504-1-054504-4.

73. Webb, P. W. (1975). Hydrodynamics and energetics of fish propulsion. *Bull. Fish. Res. Board Can.* **190**: 1–159.

74. Webb, P. W. and De Buffrénil, V. (1990). Locomotion in the biology of large aquatic vertebrates. *Trans. Am. Fish. Soc*. **119**: 629-641.

766 75. Wickham et al., (2019). Welcome to the Tidyverse. *J. Open Source Software* **4**: 1686.
767 76. Williams, T. M. (1999). The evolution of cost efficient swimming in marine mammals:
768 Limits to energetic optimization. *Phil. Trans.Roy. Soc. Lond. B* **354**:193–201.
769 77. Williams, T. M., Friedl, W. A., and Haun, J. (1993). Balancing power and speed in
770 bottlenose dolphins (*Tursiops truncatus*). *Symp. Zool. Soc. Lond*. 66: 383-394.
771 78. Williamson, G. R. (1972). The true body shape of rorqual whales. *J. Zool., Lond*. **167**:
772 277-286.
773 79. Woodward, B. L., Winn, J. P. and Fish, F. E. (2006). Morphological specializations of
774 baleen whales associated with hydrodynamic performance and ecological niche. *J.*
775 *Morph*. ***267***: 1284-1294.
776 80. Wyrick, R. F. (1954). Observations on the movements of the Pacific gray whale
777 *Eschrichtius robustus* (Cope). *J. Mamm*. **35**: 596-598.
778 81. Yates, G. T. (1983). Hydrodynamics of body and caudal fin propulsion. In *Fish*
779 *Biomechanics* (ed. P. W. Webb and D. Weihs), pp. 177–213. New York: Praeger.
780 82. Yazdi, P., Kilian, A. and Culik, B. (1999). Energy expenditure of swimming bottlenose
781 dolphins (*Tursiops truncatus*). *Mar. Biol*. **134**; 601-607.
782

Tables/Figures/Legends

		Kinematics				***Morphometrics***				
Species	***Number of Individuals***	***Swim Speed (Routine) (m s^{-1})***	***Oscillatory Frequency (Routine) (Hz)***	***Swim Speed (Lunge) (m s^{-1})***	***Oscillatory Frequency (Lunge) (Hz)***	***Total Length (m)***	***Wetted Surface Area (m^2)***	***Body Mass (kg)***	***Chord Length (m)***	***Fluke Area (m^2)***
Humpback	31 (30)	2.15 ± 0.066	0.24 ± 0.006	2.85 ± 0.100	0.34 ± 0.011	11.09 ± 0.33	61.50 ± 1.80	20537.85 ± 1363.54	1.05 ± 0.03	3.14 ± 0.18
Blue	18	2.27 ± 0.063	0.19 ± 0.004	3.05 ± 0.056	0.24 ± 0.004	22.50 ± 0.32	152.50 ± 2.20	67301.16 ± 3172.36	1.29 ± 0.03	4.71 ± 0.18
Antarctic Minke	14	2.44 ± 0.053	0.40 ± 0.010	2.96 ± 0.117	0.49 ± 0.008	7.30 ± 0.34	25.54 ± 1.21	5528.91 ± 450.57	0.55 ± 0.03	0.77 ± 0.06
Bryde's	2	1.76 ± 0.51	0.25 ± 0.005	3.11 ± 0.629	0.42 ± 0.01	12.04 ± 2.07	51.32 ± 16.39	11737.54 ± 5193.87	0.81 ± 0.13	1.97 ± 0.56
Fin	2	3.02 ± 0.125	0.25 ± 0.015	3.61 ± 0.900	0.32 ± 0.018	18.90 ± 0.43	109.90 ± 2.50	39515.13 ± 2330.65	1.07 ± 0.07	2.78 ± 0.35
Sei	1	2.23	0.22	2.46	0.30	16.62	92.71	27275.04	1.15	3.23

Table 1. Kinematic and morphometric variables used for modeling of hydrodynamic properties for all (n=63) individual whales in our dataset. Those with an asterisk were modeled using available data and methods in the literature. All values are given as the mean ± the standard error.

Oscillatory Frequency (Hz) vs. Total Length (m) (Figure 3)	*Linear equation*	*R2*	*P – value*
Routine Effort Swimming	$\hat{y} = -0.560x + 0.313$	0.77	<0.001
Lunge-Associated Swimming	$\hat{y} = -0.565x + 0.009$	0.76	<0.001
Swim Speed (m s^{-1}) vs. Total Length (m) (Figure 3)			
Routine Effort Swimming	$\hat{y} = -0.003x + 0.785$	$6.25*10^{-5}$	0.949
Lunge-Associated Swimming	$\hat{y} = 0.078x + 0.873$	0.04	0.098
***Mean Mass-Specific Thrust Power vs. Swim Speed (m s^{-1})* (Figure 4)**			
Routine Effort Swimming	$\hat{y} = 0.731x – 2.764$	0.40	< 0.001
Lunge-Associated Swimming	$\hat{y} = 0.630x – 2.138$	0.49	< 0.001
Mean Mass-Specific Thrust Power vs. Total Length (Figure 4)			
Routine Effort Swimming	$\hat{y} = 0.033x – 1.594$	0.23	< 0.001
Lunge-Associated Swimming	$\hat{y} = 0.031x – 0.693$	0.16	< 0.001
Drag Coefficient vs. Swim Speed (m s^{-1}) (Figure 5)			
Routine Effort Swimming	$\hat{y} = -0.613x – 2.617$	0.12	0.004
Lunge-Associated Swimming	$\hat{y} = -0.270x – 3.148$	0.06	0.042
Drag Coefficient vs. Total Length (m) (Figure 5)			
Routine Effort Swimming	$\hat{y} = 0.082x – 5.080$	0.64	<0.001
Lunge-Associated Swimming	$\hat{y} = 0.058x – 4.737$	0.41	<0.001
Drag Coefficient vs. Reynolds Number (Figure 5)			
Routine Effort Swimming	$\hat{y} = 2.92*10^{-8}x – 4.805$	0.41	<0.001
Lunge-Associated Swimming	$\hat{y} = 1.36*10^{-8}x – 4.476$	0.23	<0.001
Froude Efficiency vs. Total Length (m) (Figure 6)			
Routine Effort Swimming	$\hat{y} = -0.004x – 0.049$	0.68	< 0.001
Lunge-Associated Swimming	$\hat{y} = -0.003x – 0.068$	0.47	< 0.001

812

813 Table 2. This table contains equations, estimates, R^2 values, and p values from generalized linear
814 mixed models for sequential figures 3-7 and 9.

Hydrodynamic Calculations

Species	*Mass-Specific Thrust Power (Watts kg^{-1})*	*Drag Coefficient*	*Reynolds Number*	*Froude Efficiency*
Humpback	0.30 ± 0.023	0.02 ± 0.002	2.29×10^7 ± 9.9×10^5	0.908 ± 0.003
Blue	0.48 ± 0.025	0.04 ± 0.006	4.89×10^7 ± 1.3×10^6	0.860 ± 0.006
Antarctic Minke	0.36 ± 0.028	0.01 ± 0.001	1.71×10^7 ± 9.9×10^5	0.920 ± 0.004
Bryde's	0.50 ± 0.213	0.04 ± 0.012	2.13×10^7 ± 9.4×10^6	0.868 ± 0.022
Fin	0.74 ± 0.130	0.02 ± 0.007	5.46×10^7 ± 1.0×10^6	0.889 ± 0.018
Sei	0.51	0.03	3.54×10^7	0.876

Table 3. Results from hydrodynamic and morphometric calculations for all individuals (n=63) from each species. All values are given as the mean of all tailbeats in a deployment ± the standard error. The drag coefficient, Reynolds number, and Froude efficiency are dimensionless. The mean fluke area is shown in m^2 and the chord length and total length are shown in meters.

Species	*Swim Speed (m s^{-1}) or (bl s^{-1})**	*Total Length (m)*	*Froude Efficiency*	*Source(s)*
Homo sapien *Human (Female)*	0.95	2.38	0.29	von Loebbecke et al., 2009
Ondatra zibethicus *Muskrat*	0.75	0.44	0.33	Fish, 1984
Pterophyllum eimekei *Freshwater Angelfish*	0.04	0.08	0.16	Blake, 1979; Blake, 1980
Danio rerio *Zebra Danio*	Multiple	0.0315	0.80	McCutchen, 1975
Cymatogaster aggregata *Shiner Perch*	0.57	0.143	0.65	Webb, 1975
Oncorhynchus mykiss *Rainbow Trout*	U_{crit}	0.293	0.75	Webb, 1975
Euthynnus affinis *Mackerel Tuna (Kawakawa)*	1.52	0.40	0.90	Magnuson, 1978
Pusa hispida *Ringed Seal*	0.75	1.03	0.88	Fish et al., 1988
Pagophilus groenlandicus *Harp Seal*	1.04	1.43	0.87	Fish et al., 1988
Trichechus manatus *American Manatee*	0.30*	3.23	0.83	Kojeszewski and Fish, 2007
Delphinapterus leucas *Beluga Whale*	3.00	3.64	0.84	Fish 1998
Lagenorhynchus obliquidens *Pacific White-Sided Dolphin*	5.30	2.00	0.89	Webb, 1975; Yates, 1983; Blickhan and Cheng, 1994

Orcinus orca *Killer Whale*	6.50	4.74	0.88	Fish, 1998
Pseudorca crassidens *False Killer Whale*	3.80	3.75	0.90	Fish, 1998
Sotalia guianensis *Guiana Dolphin*	2.40	1.90	0.83	Blickhan and Cheng, 1994
Tursiops truncatus *Common Bottlenose Dolphin*	2.40[1], 3.80[2]	2.50[1], 2.61[2]	0.78[1], 0.86[2]	Blickhan and Cheng, 1994[1]; Fish, 1998[2]
Balaenoptera physalus *Fin Whale*	3.02 ± 0.125 (Routine Effort Swimming)	18.90 ± 0.43	0.899 ± 0.018	Current Study
Balaenoptera bonaerensis *Antarctic Minke Whale*	2.44 ± 0.053 (Routine Effort Swimming)	7.30 ± 0.34	0.920 ± 0.004	Current Study
Megaptera Novaeangliae *Humpback Whale*	2.15 ± 0.066 (Routine Effort Swimming)	11.09 ± 0.33	0.908 ± 0.003	Current Study
Balaenoptera musculus *Blue Whale*	2.27 ± 0.063 (Routine Effort Swimming)	22.50 ± 0.32	0.860 ± 0.006	Current Study
Balaenoptera borealis *Sei Whale*	2.23 (Routine Effort Swimming)	16.62	0.876	Current Study
Balaenoptera brydei *Bryde's Whale*	1.76 ± 0.51 (Routine Effort Swimming)	12.04 ± 2.07	0.868 ± 0.022	Current Study

Table 4. Froude efficiency and metadata collected from various sources for the creation of figure 8.

Figure 1. Adaptation from Shadwick (2005) showing the forces acting on the tail of a thunniform swimmer such as a blue whale during active oscillatory fluking of the tail. The heaving motion of the tail creates a pressure imbalance between the top and bottom faces of the fluke that results in the generation of a lift force perpendicular to the path of the flukes and a thrust force in the forward direction of travel of the animal.

Figure 2. Representative UAS drone image of a humpback whale showing the morphometric measurements taken from each animal. The white line corresponds to the total length (in meters) from the tip of the lower jaw to the caudal midpoint of the tail. The chord length of the fluke (in meters) is denoted by the red line running from the cranial insertion of the fluke onto the peduncle to the caudal midpoint of the tail. The purple shaded region corresponds to the tail area (in m^2) comprising the entirety of the flukes and the peduncle region caudal to the cranial fluke insertions. Make lines thicker.

Figure 3. Linear regressions showing the $\log^{10}$ of total body length (m) versus the A) oscillatory frequency (Hz) and B) swim speed (m s^{-1}) for both routine swimming (solid line) and lunge-associated swimming (dashed line). Each point corresponds to the mean value for a single individual whale and a single swimming mode (● circle: routine; ▲ triangle: lunge-associated).

Figure 4. Linear regressions showing A) swim speed (m s^{-1}) and B) total body length (m) versus mass-specific thrust power output (W kg^{-1}) for both routine swimming (solid line) and lunge-associated swimming (dashed line). Each point corresponds to the mean value for a single individual whale and a single swimming mode (● circle: routine; ▲ triangle: lunge-associated). One point was removed above the visual range of each figure (Bryde's whale: mean swim speed = 3.74 m s^{-1}; total body length = 14.1 m; mean mass-specific thrust power output = 2.60 Watts kg^{-1}).

Figure 5. Linear regressions showing A) swim speed (m s^{-1}), B) total body length (m), and C) Reynolds number (dimensionless) versus the drag coefficient (dimensionless) for both routine swimming (solid line) and lunge-associated swimming (dotted line). Each point corresponds to the mean value for a single individual whale and a single swimming mode (● circle: routine; ▲ triangle: lunge-associated). One point was removed above the visual range of each figure (blue whale: mean swim speed = 1.68 m s^{-1}; total body length = 24.1 m; mean Reynolds number = 3.9e+07; mean drag coefficient = 0.131).. Dot-dash lines shown in C) are linear regressions of Reynolds number versus drag coefficient for simple rigid-body model comparison using equations derived from Hoerner (1965). Illustration shows a swimming blue whale and image shows an R100 rigid-body as visual representations of the data shown in C).

Figure 6. Curved fit lines showing A) swim speed (m s^{-1}) and linear regressions showing B) total body length (m) versus propulsive efficiency (dimensionless) for both routine swimming (solid line) and lunge-associated swimming (dotted line). Curved fit lines are shown in A) to better illustrate the effects of maximal performance on Froude efficiency, and each point in B) corresponds to the mean value for a single individual whale and a single swimming mode (● circle: routine; ▲ triangle: lunge-associated). Plots along x-axis of A) shows the density of swim speeds for routine (solid border) and lunge-associated swimming (dotted border). One point was

882 removed above the visual range of each figure (Bryde's whale: mean swim speed = 3.74 m s^{-1};
883 total body length = 14.1 m; mean mass-specific thrust power output = 2.60 Watts kg^{-1}).
884
885 Figure 7. Propulsive efficiency versus total body length (m) for species from different
886 morphological and taxonomic groups and use different swimming modes (● circle: drag-based
887 paddling; ▲ triangle: undulatory swimming; ■ square: oscillatory swimming). The mysticete
888 cetaceans are the mean species-level data from our present study. Silhouettes correspond to each
889 group by rough position and color.

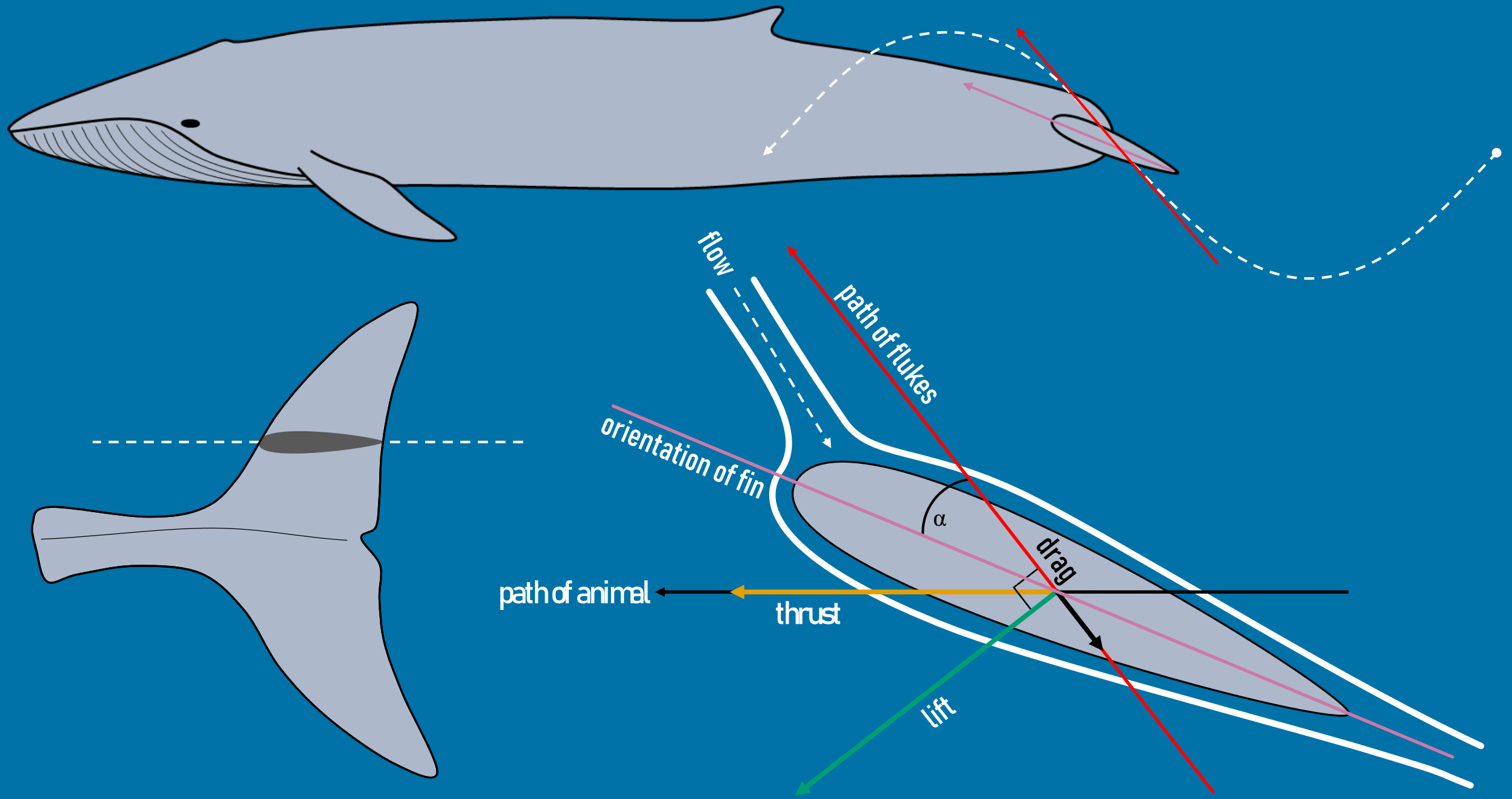
flow
path of flukes
orientation of fin
α
drag
path of animal
thrust
lift

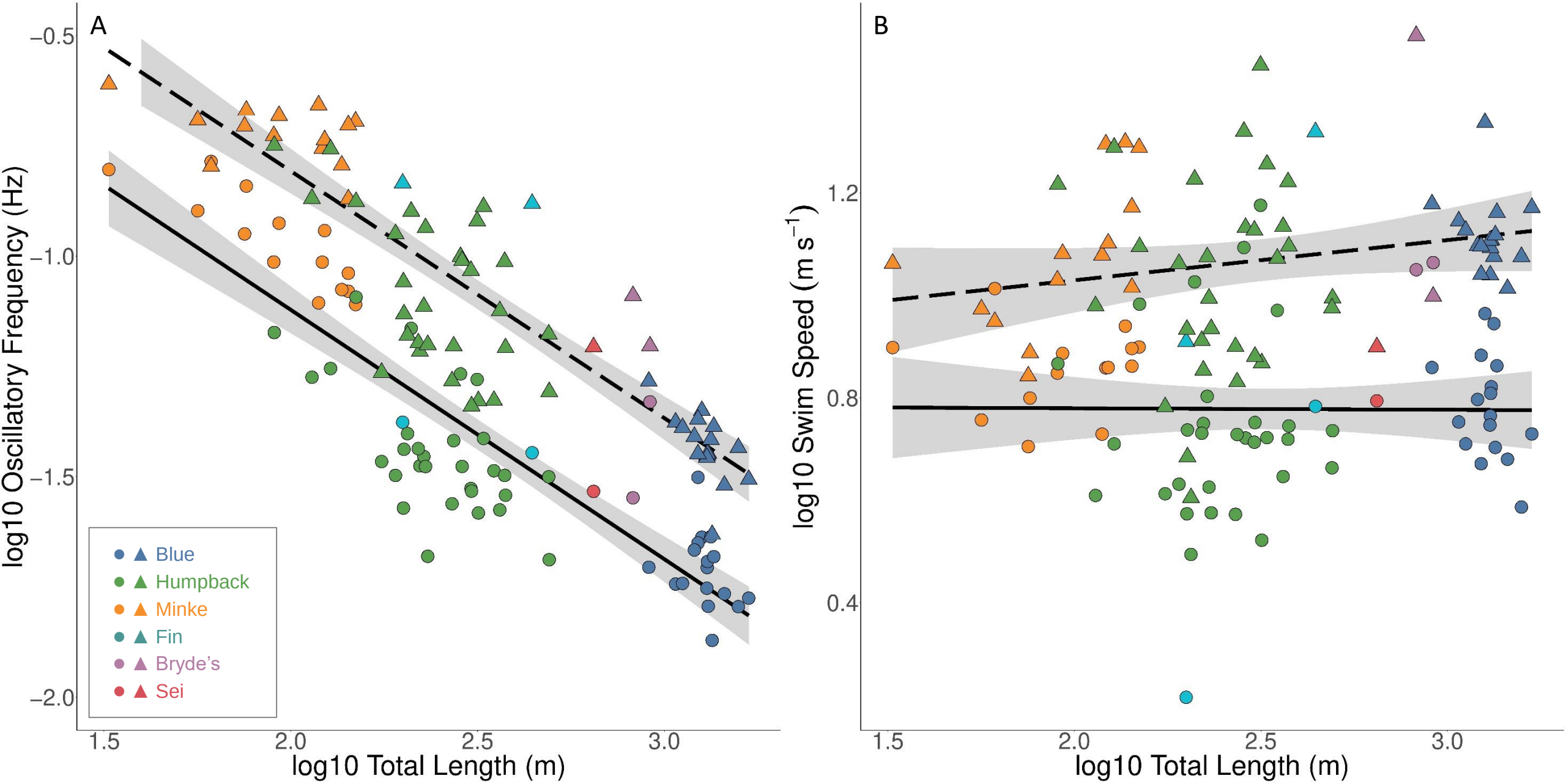
A
B
log10 Oscillatory Frequency (Hz)
log10 Swim Speed (m s^{-1})
log10 Total Length (m)
log10 Total Length (m)
−0.5
−1.0
−1.5
−2.0
1.2
0.8
0.4
1.5
2.0
2.5
3.0
Blue
Humpback
Minke
Fin
Bryde's
Sei

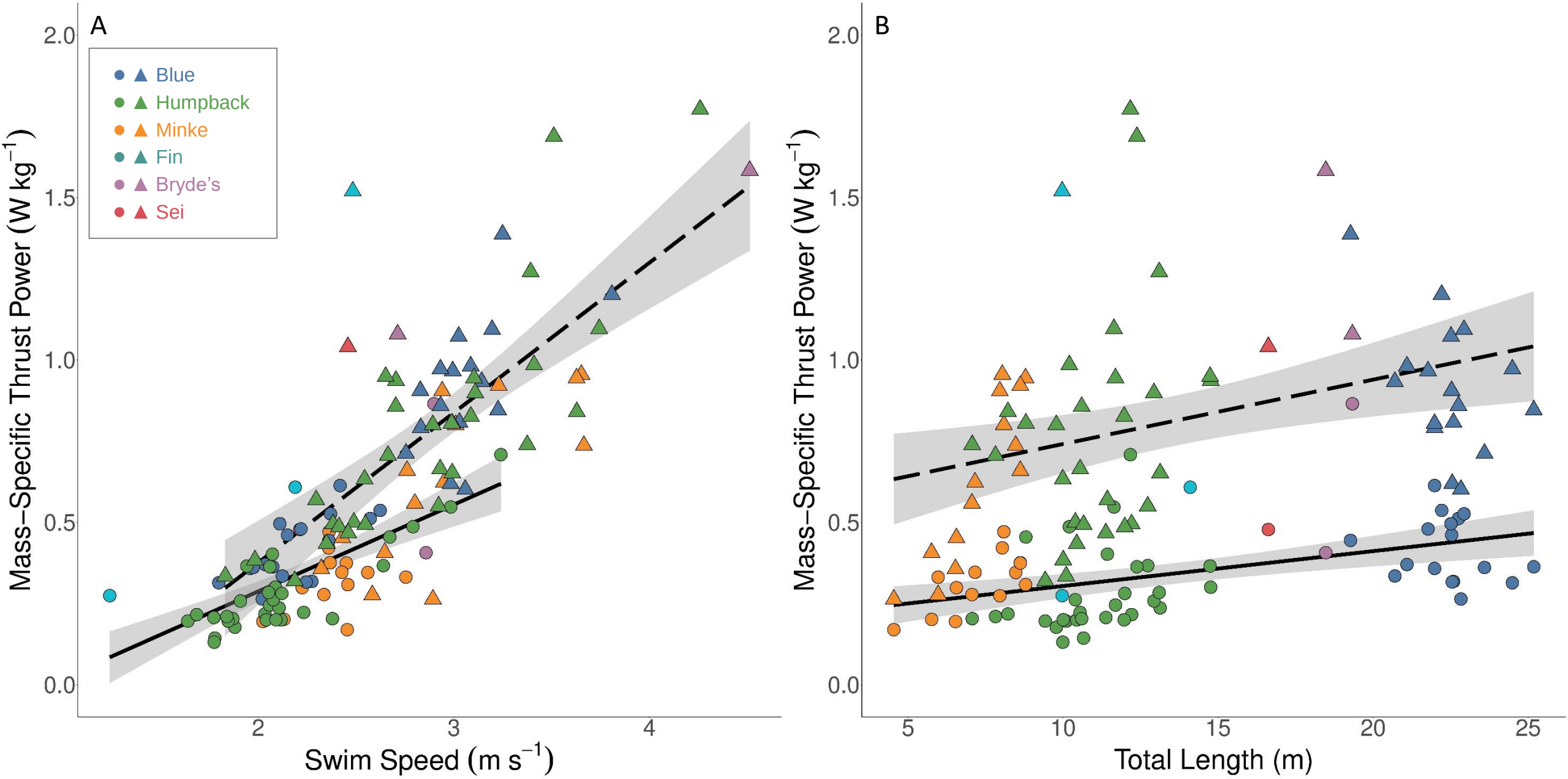
A
B
Blue
Humpback
Minke
Fin
Bryde's
Sei
Mass–Specific Thrust Power (W kg^{-1})
Swim Speed (m s^{-1})
Total Length (m)
0.0
0.5
1.0
1.5
2.0
2
3
4
5
10
15
20
25

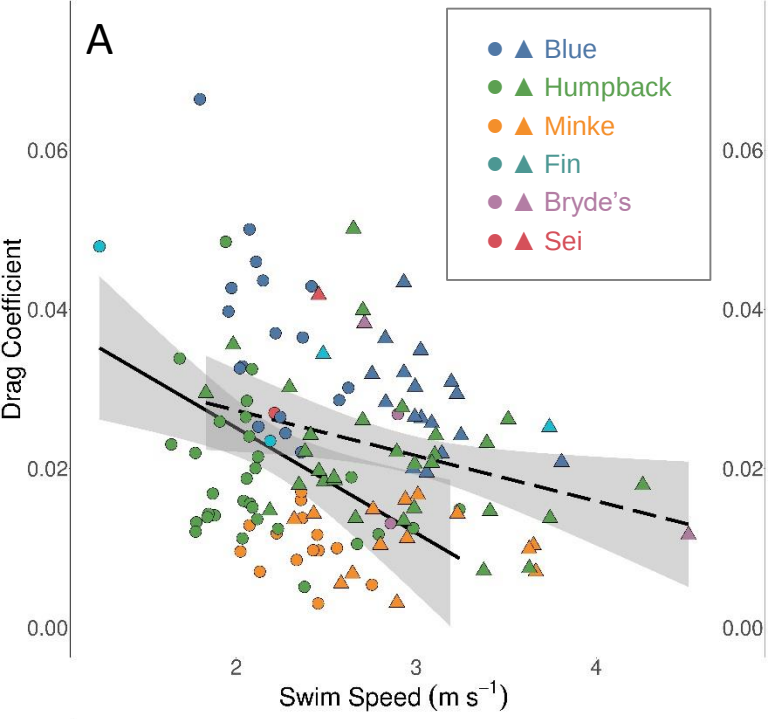

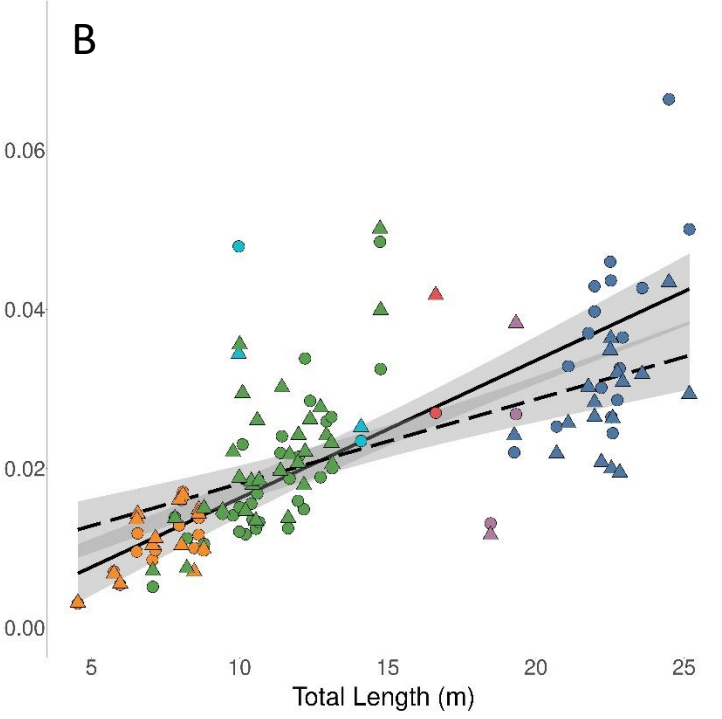

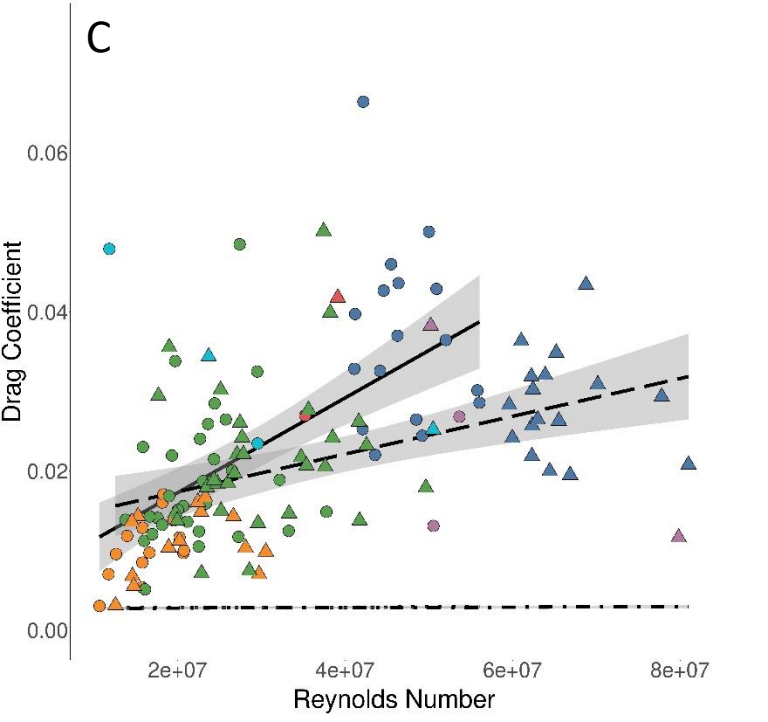

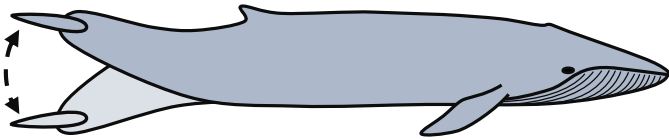

Whale: Control surfaces intact and active fluking

R100 Model: Control surfaces removed and non-fluking travel

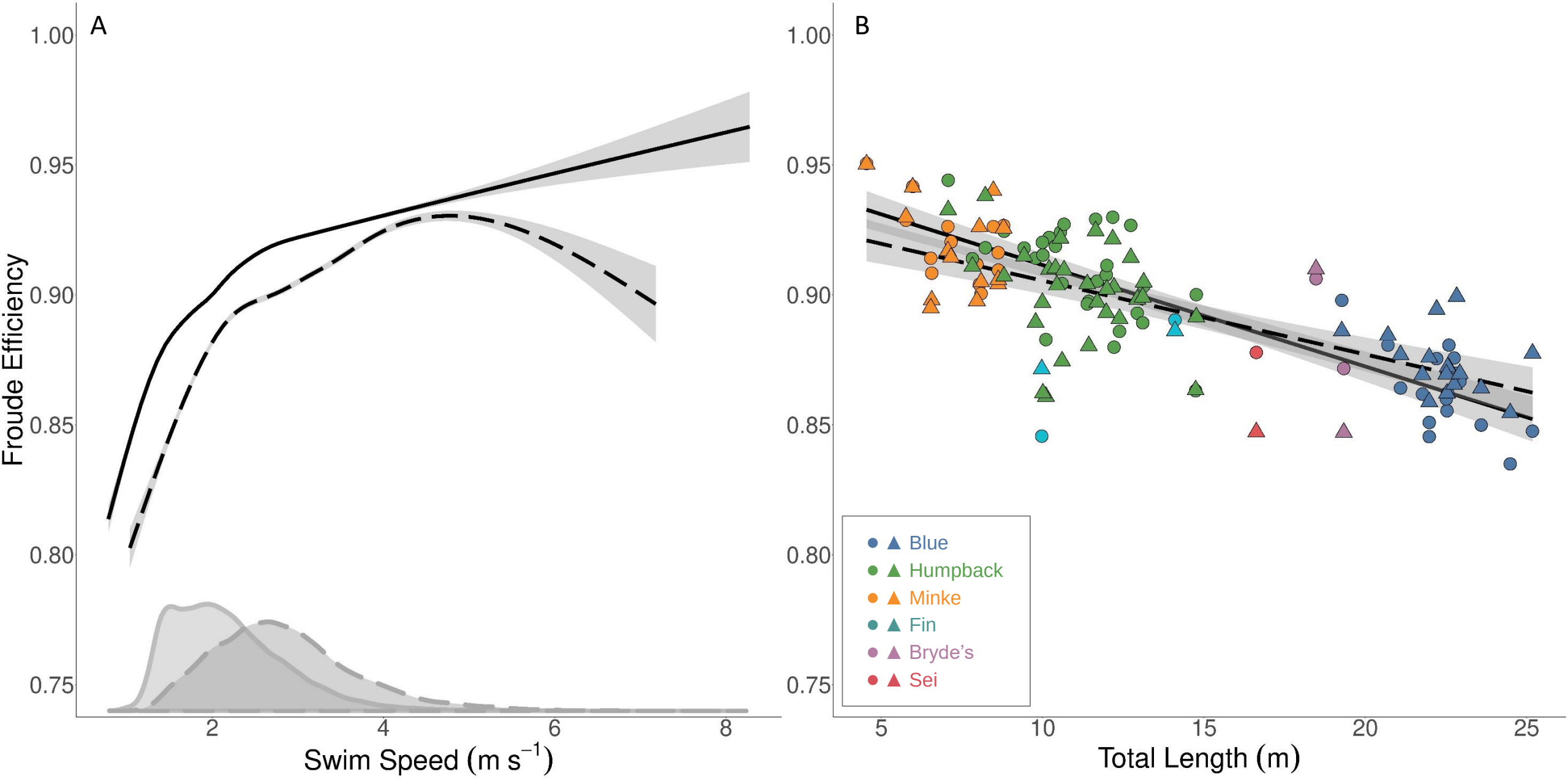
A
B
1.00
0.95
0.90
0.85
0.80
0.75
Froude Efficiency
2
4
6
8
Swim Speed (m s^{-1})
5
10
15
20
25
Total Length (m)
Blue
Humpback
Minke
Fin
Bryde's
Sei

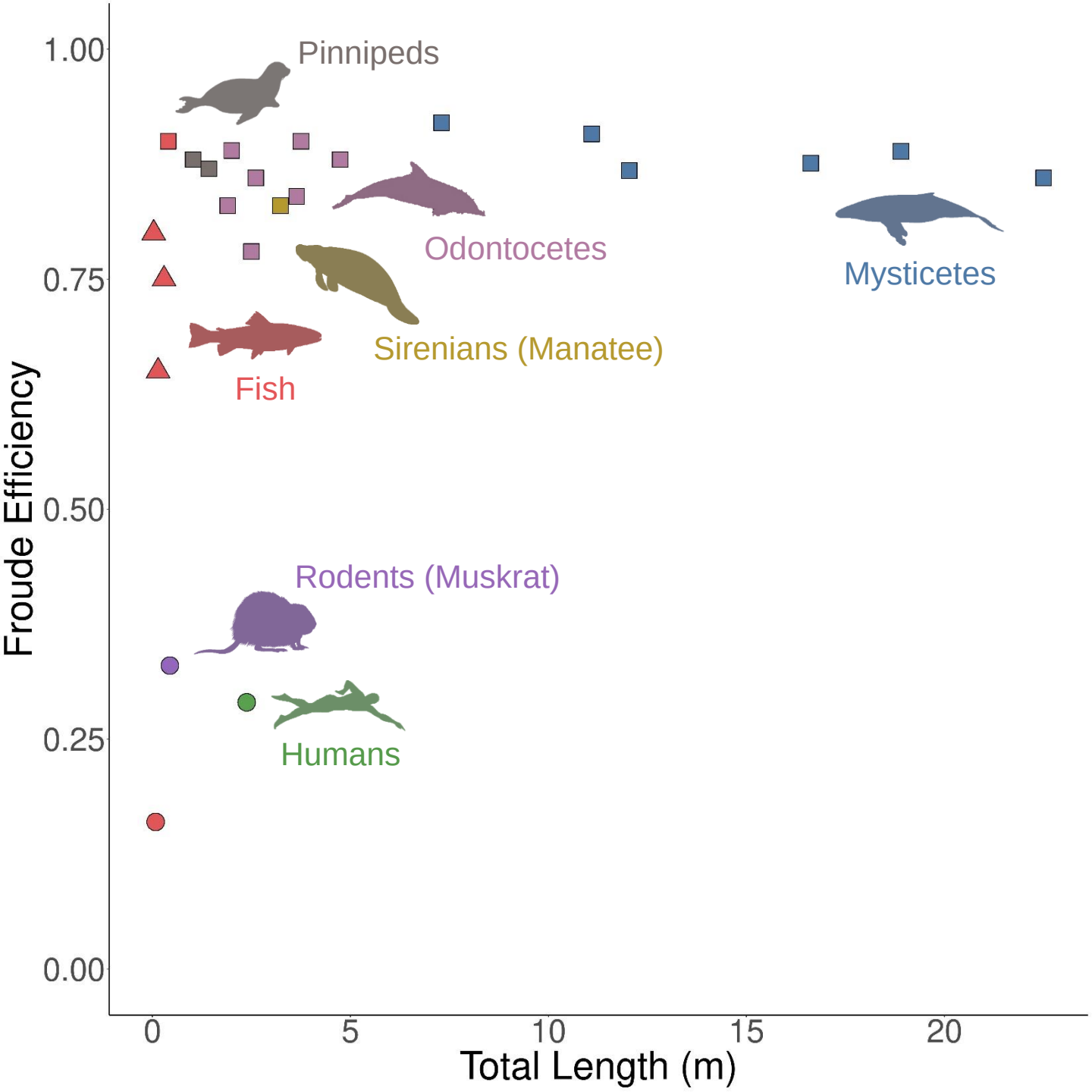
Pinnipeds
Odontocetes
Mysticetes
Sirenians (Manatee)
Fish
Rodents (Muskrat)
Humans
1.00
0.75
0.50
0.25
0.00
Froude Efficiency
0
5
10
15
20
Total Length (m)